Proceedings of the Third SPREP Meeting on Climate Change and Sea Level Rise in the South Pacific Region.
Noumea, New Caledonia, 18–22 August 1997.

ON SEA LEVEL CHANGES IN THE TROPICAL PACIFIC DURING EL NIÑO–SOUTHERN OSCILLATION EVENTS

Thierry Delcroix and Pierre Rual

SURTROPAC Group
ORSTOM
New Caledonia

INTRODUCTION

The tropical Pacific ocean encompasses about half the circumference of the earth at the equator, and it is subject to dramatic climate variability on an interannual time scale: the El Niño–Southern Oscillation (ENSO) phenomenon. Two valuable sources of information for monitoring, understanding and ultimately predicting the ENSO-related effects are the Volunteer Observing Ship (VOS) eXpandable BathyThermograph (XBT) network (White *et al.*, 1985), and the Tropical Atmosphere Ocean (TAO) buoy array (Hayes *et al.*, 1991; McPhaden, 1993).

Among its notable climatic effects, ENSO is concerned with dramatic sea level changes which are particularly of interest for the Pacific islands due to their physiographic, ecological, socio-economic and cultural characteristics. Relying mainly on the VOS-XBT and TAO observing systems, this note aims to document the ENSO-related sea level changes for the whole tropical Pacific, and for the 1979–1996 period which covers numerous El Niño and La Niña events. Sea level changes are inferred from 0/450 dbar dynamic height anomalies, given the excellent accord between sea level and surface dynamic height variations in the tropical Pacific (Rébert *et al.*, 1985). Hereafter, the terms "0/450 dbar dynamic height anomaly" and "sea level" are used interchangeably.

DATA AND METHODS

Surface Dynamic Height Anomaly

Computation. About 250 000 temperature profiles were collected in the tropical Pacific during 1979–1996. After validation tests (not detailed here), the irregularly distributed temperature data, both in space and time, were gridded onto bi-monthly field with a resolution of 1° latitude by 5° longitude. The gridding procedure was performed through an objective analysis routine (courtesy of P. deMey) in which the spatial and temporal decorrelation scales were based on Meyers *et al.* (1991). For each grid point, the temperature profile was converted into 0/450 dbar dynamic height anomaly using local mean T-S curves from Levitus *et al.* (1994). The time variability of T-S curves which can result in local signals of as much as 5dyn cm in surface dynamic height (e.g. Delcroix *et al.*, 1987) was not considered, as we lacked time series in salinity profiles.

Mean, Standard Deviation, and Error. In order to set the context, figure 1 presents the 1979–1996 averaged 0/450 dbar dynamic height anomaly, its standard deviation and its estimated normalised error. The main relief (figure 1a) consists of: a) the existence of a well-marked zonal slope in the equatorial band with a 40 dyn cm difference between the eastern and western basin; and, b) almost zonally oriented ridges and troughs which mark the meridional boundaries of the mean surface geostrophic currents. This mean map is in general agreement with previous studies (e.g. Reid, 1961). The standard deviation in sea level (Figure 1b) presents values in excess of 6cm in the equatorial band, with maximum values in the west specially for two patches centered near 5°N and 5°S latitudes (>10cm). The mean error (figure 1c) roughly mirrors the distribution of available data along ship tracks (the contribution of TAO measurements weakly shows up as they are only available from 1992 on). Statistical tests (not detailed here) indicate that values having an error greater than 0.8 should be view with great care.

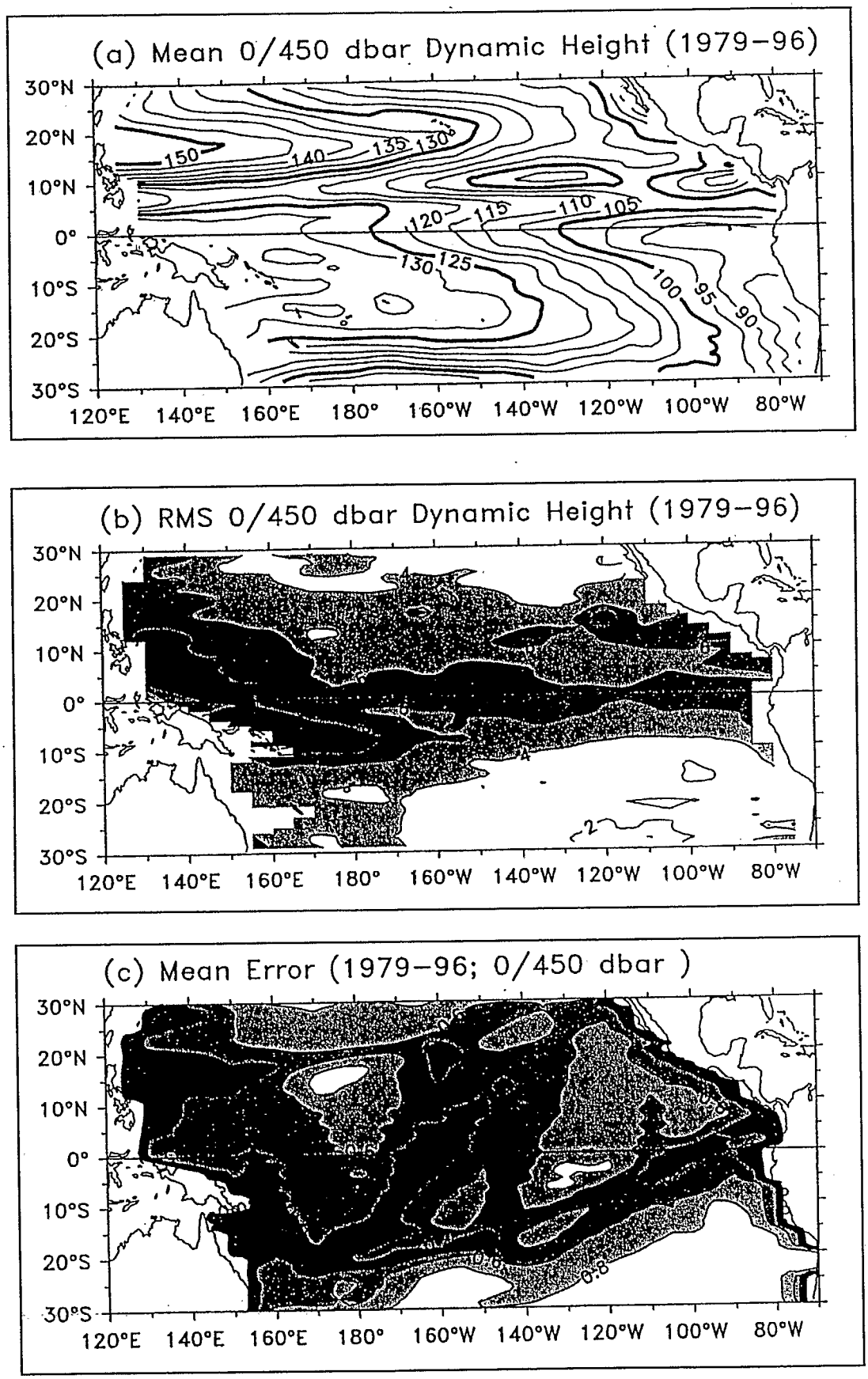

Figure 1. a) mean (dyn cm), b) standard deviation (dyn cm), and c) estimated normalised error of the 0/450 dbar dynamic height anomaly.

Surface Wind and Southern Oscillation Index

The surface wind was obtained from the monthly 2°latitude by 2°longitude FSU (Florida State University) pseudo wind-stress product (Goldenberg and O'Brien, 1981). The zonal and meridional components were used to compute the wind-stress curl with a centered differencing method, and the curl was sub-sampled bi-monthly onto a 1°-latitude by 5°-longitude grid. The SOI to be used is the CAC version (as detailed in the March 1986 issue of the Climate Diagnostic Bulletin), which is similar to the SOI used by Trenberth (1984) with an additional normalisation resulting in a time series having a 1951–1980 mean of zero and a variance of one.

Computation of ENSO-related Variations

The interannual variations in sea level and wind stress curl were estimated by filtering the bi-monthly time series with a 13 bi-month Hanning filter (Blackman and Tukey, 1958). This filter passes almost no signal at periods of one year and shorter, and passes about 90% of the signal at periods of 4 years which is the mean El Niño return interval (Enfield and Cid, 1991). An Empirical Orthogonal Function (EOF) was performed on these interannual variations in order to extract the ENSO-related variations which are presented in the following section.

ENSO-RELATED SEA LEVEL CHANGES

The Mode 1 EOF

Two EOF were necessary to extract the interannual variability associated with ENSO. Starting with the first EOF, Figure 2a shows a near-perfect correlation between the EOF time function and the filtered SOI. The prominent feature in the spatial pattern is the presence of positive values in the west and negative values in the east. This means that during El Niño events (1982–83, 1987, 1991–94) the sea level was lower than average in the western half of the basin, whereas it was higher than average in the eastern half; the reverse situation was observed during La Niña events (1988–89). This results in a somewhat zonal "seesaw" structure almost in phase with the SOI, with a "fulcrum" near 170°W. Such a "seesaw" was already documented from observations (Wyrtki, 1977; Chao *et al.*, 1993) and model results (Busalacchi and O'Brien, 1981; Zebiak and Cane, 1987).

Along the equator, the zonal "seesaw" is consistent with linear theory (Sverdrup, 1947) describing the equilibrium at the ENSO time scale between zonal slope in sea level and zonal wind. This equilibrium is pictured in figure 3, illustrating the excellent accord between the interannual variations of the zonal means (130°E–80°W) in sea level slope, estimated by a linear regression, and in zonal wind. This near equilibrium relationship was also verified at the annual time scale from mooring data in the eastern equatorial basin during 1983–86 (McPhaden and Taft, 1988).

Figure 2a also indicates that the meridional scale of the zonal "seesaw" is greater in the western than in the eastern half of the basin (compare the 0.02 and -0.02 isolines). Figures 4a and 4b further indicate the tendency for sea level changes to present two relative off-equatorial maxima in the west (near 5–10° latitudes) in contrast with an equatorially trapped Gaussian shape maximum in the east. This specific spatial distribution, consistent with the results of Chao and Philander (1993; see their figure 17), reflects the role of the wind stress curl at the ENSO time scale. As shown in figure 2c, the ENSO-related EOF in the curl presents two symmetrical patches about the equator centered near 7°N and 7°S in the western half of the basin, with no ENSO signals in the eastern half. The Ekman pumping associated with these two patches elevates (depresses) the thermocline during El Niño (La Niña). The resulting opposite vertical displacements in sea level are in phase with the equatorial displacement due to the zonal wind, yielding a large band of upward (La Niña) and downward (El Niño) movements of sea level at the ENSO time scale in the western half of the basin.

One must be cautious in using the term zonal "seesaw" suggested by the EOF analysis, as it is not a rigid "seesaw". As a matter of fact, low frequency variations in sea level are depicted in figures 5a and 5b, in physical units, for two points at the equator in the western (155°E) and eastern (100°W) basin. These variations, of the order of 25cm, clearly illustrate that the eastern and western sea level anomalies are not exactly opposite in phase: the maximum correlation R=-0.87 between the two time series is obtained when the 0–155°E sea level lags behind the one at 0–100°W by three bi-months (R=-0.69 at 0 lag). These differences in time were well-captured for heat content by a coupled model (Zebiak and Cane, 1987), and resulted chiefly from propagating equatorial Kelvin and gravest Rossby waves.

The Mode 2 EOF

The second EOF in sea level also extracts an ENSO-like signal (figure 2b). The time function

compares well with the filtered SOI, with a maximum correlation coefficient obtained when it lags behind the SOI by about one year. The spatial

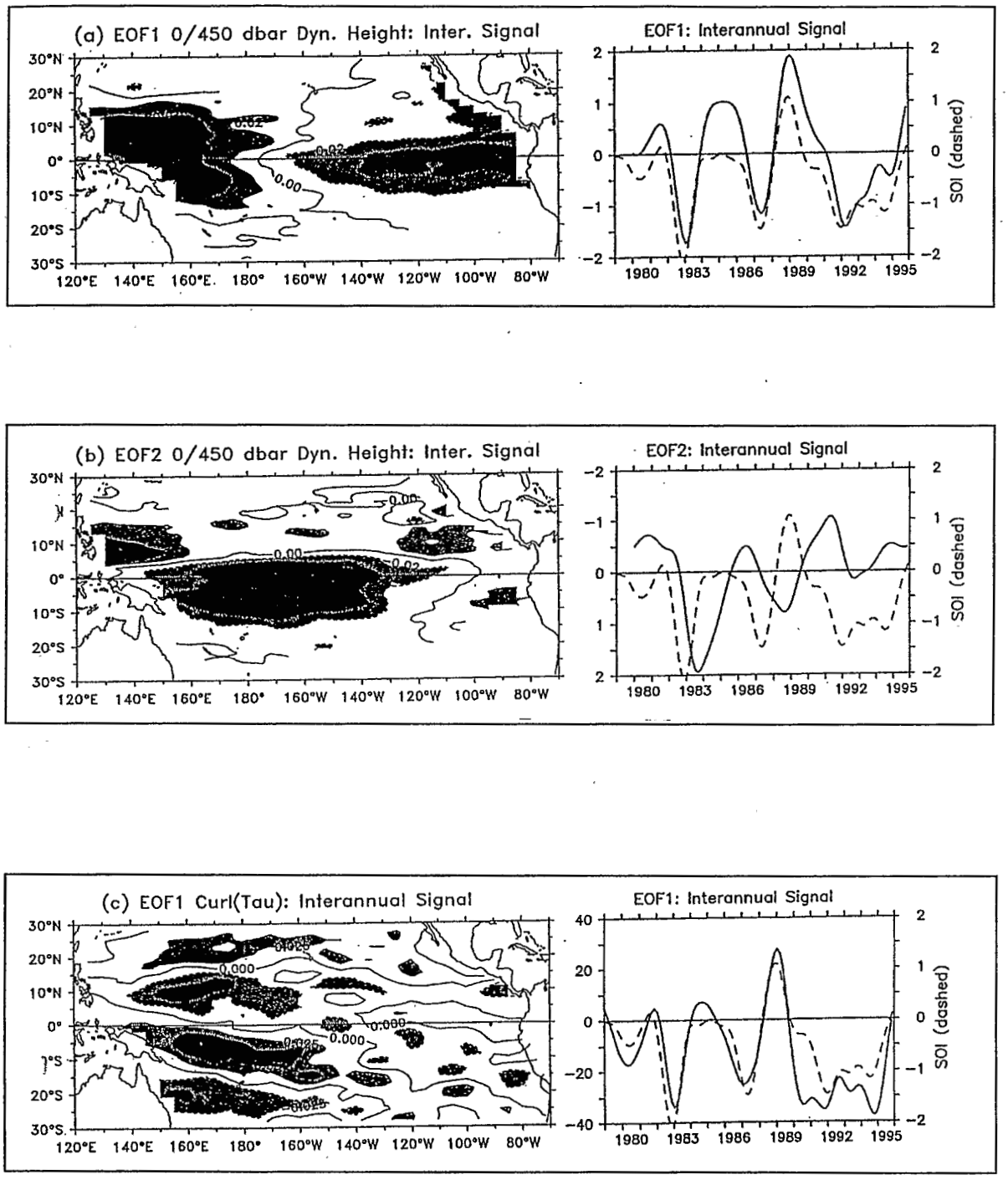

Figure 2. Spatial patterns (left pamels) and time functions (right panels, full lines, left vertical axes) of the interannual a) mode 1, b) mode 2 EOF in 0/450 dbar dynamic height anomaly, and c) mode 1 EOF in pseudo wind stress curl. The dashed lines on the right panels represent the 25-month Hanning filtered SOI scaled on the right vertical axes. The units are defined so that the products between the spatial patterns and the time functions are a–b) dyn m, and c) m^2s^{-2} per 1° latitude.

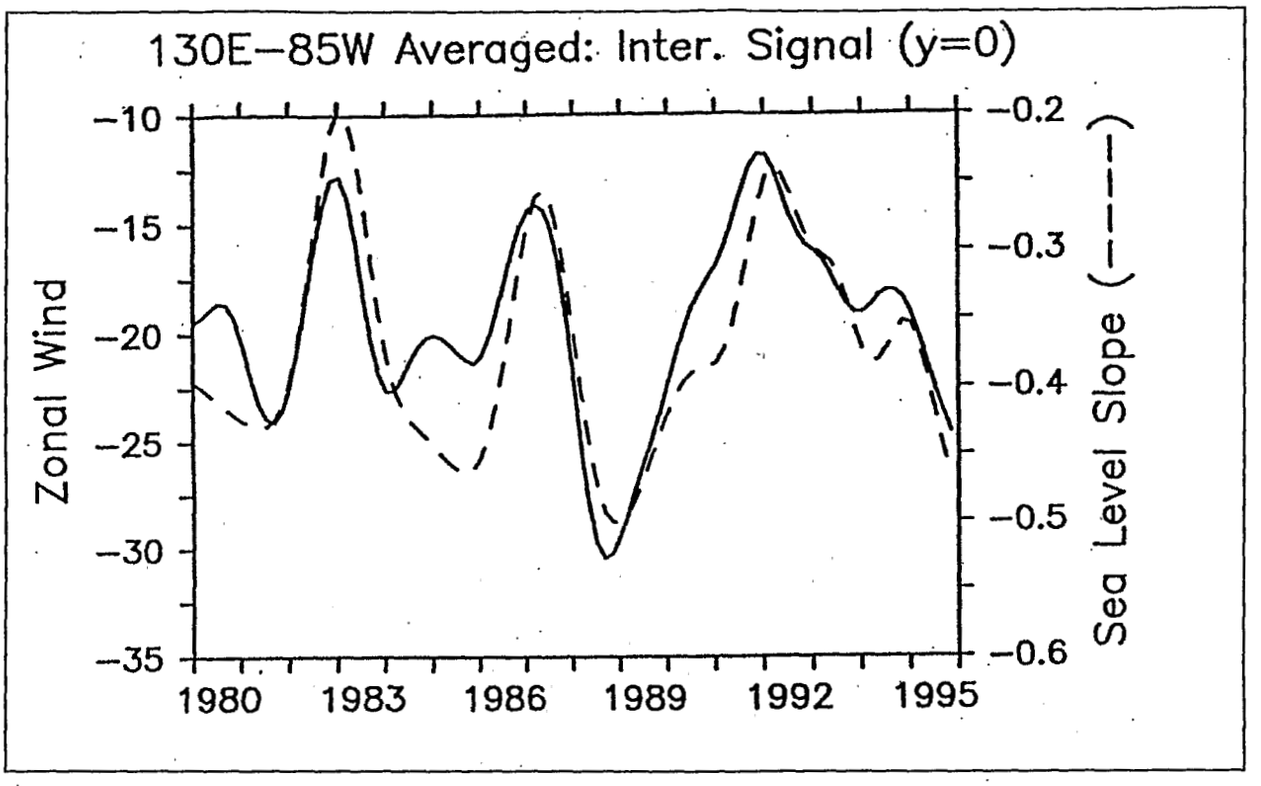

Figure 3. Interannual variations in 130°E - 80°W averaged zonal wind stress (left axis; m2s-2) and sea level slope (right axis; dyn m per 10° lonitude) at the equator.

pattern approximately separates the 20°S–5°N from the 5°N–20°N zonal strips, with maximum amplitudes in the western–central equatorial basin and nearby 8°N in the west. This EOF indicates that there is a build-up of mass up to, and not just till the beginning of, the mature phase of El Niño events within 5°N–20°S, and a mass release within 5°N–20°N (the EOF time function changes sign, from negative to positive, when the SOI is minimum). Conversely, the aftermath of an El Niño event leaves the 5°N–20°S band with a net deficit of mass, contrasting with the 5°N–20°N band which is filled up, in qualitative agreement with Wyrtki's scenario (1985).

To show this meridional "seesaw" in physical units, figures 5c–d compares the 0°–165°W and 8°N-140°E sea level time series. At 0°–165°W, there was a net mass depletion by the end of 1983, in mid-1988 and by the end of 1992, about a year after the minimum SOI values associated with the El Niño events, and a gradual mass recovery between these events. Out-of-phase sea level variations clearly occurred at 8°N–140°E with similar peak to peak sea level variations of the order of 30cm.

Zonally-integrated Sea Level Changes

Figure 4c shows the 130°E–85°W zonally-integrated sea level as a function of latitude and time, with the 1980–95 average removed. The zonal average smoothes out the east-west "seesaw", and so emphasises the meridional "seesaw". In the equatorial band (say 5°N–5°S), there is an increase of zonally-integrated sea level up to the mature phases of the El Niño events (end of 1982, early 1987 and early 1992) and a sharp decrease lasting for 1–2 years after these mature phases. The latitudes south of 5°S vary almost in phase with the equatorial band, in contrast with the latitudes north of 5°N which tend to be out-of-phase with the equatorial band. This observed zonally-integrated sea level variability is remarkably consistent with the zonally-integrated heat content variability modelled by Zebiak (1989). It suggests a mass exchange across the equator at the ENSO time scale, as recognised from sparse island sea level observations (Wyrtki, 1985) and various model simulations (Pares-Sierra *et al.*, 1985; Philander and Hurlin, 1988; Springer *et al.*, 1990; Chao and Philander, 1993).

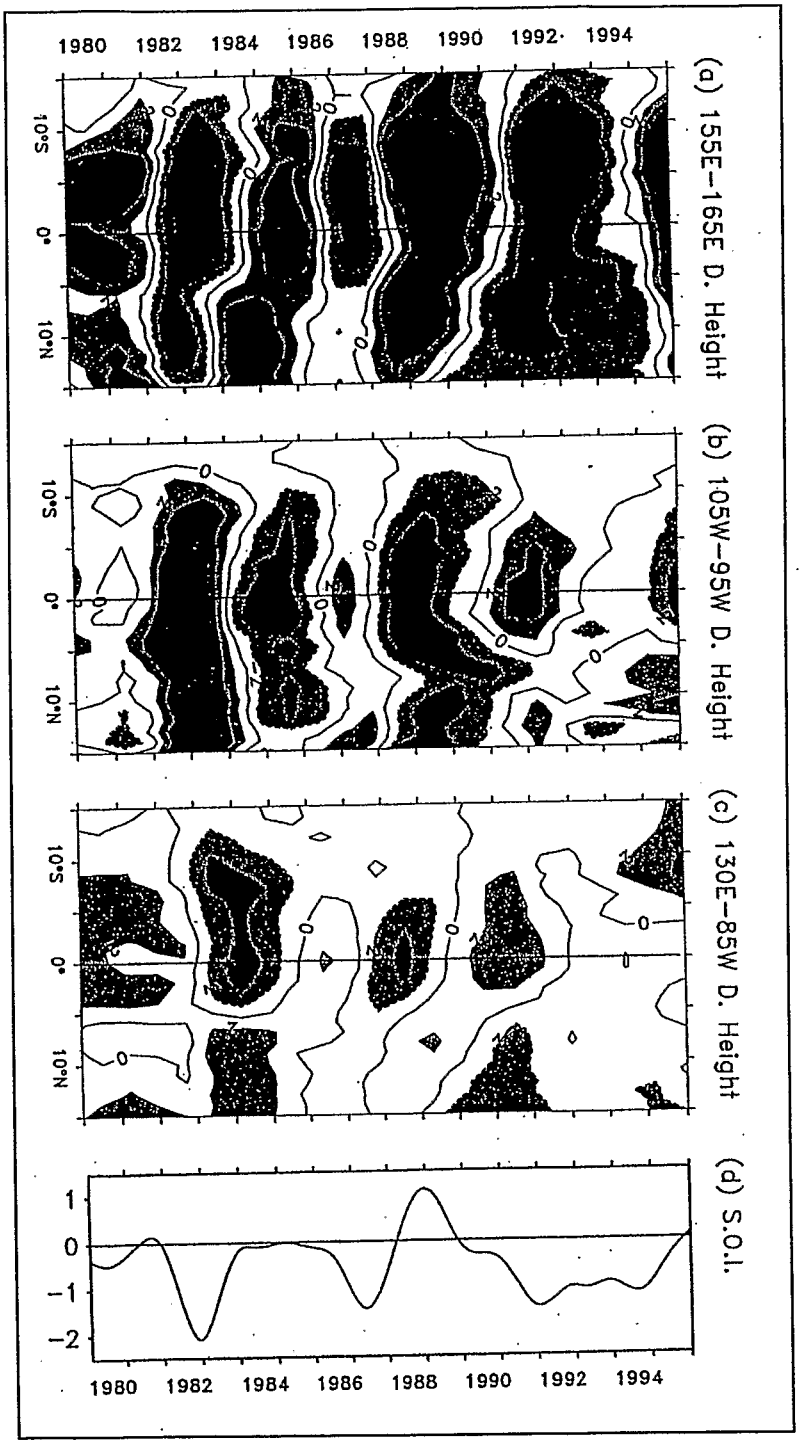

Figure 4. Latitude–time variations in 0/450 dbar dynamic height anomaly, realtive to the 1980–1995 period, averaged within a) 155°E–165°E, b) 105°W–95°W and c) 130°E–85°W. Contour interval is 2dyn cm. The right panel is the SOI.

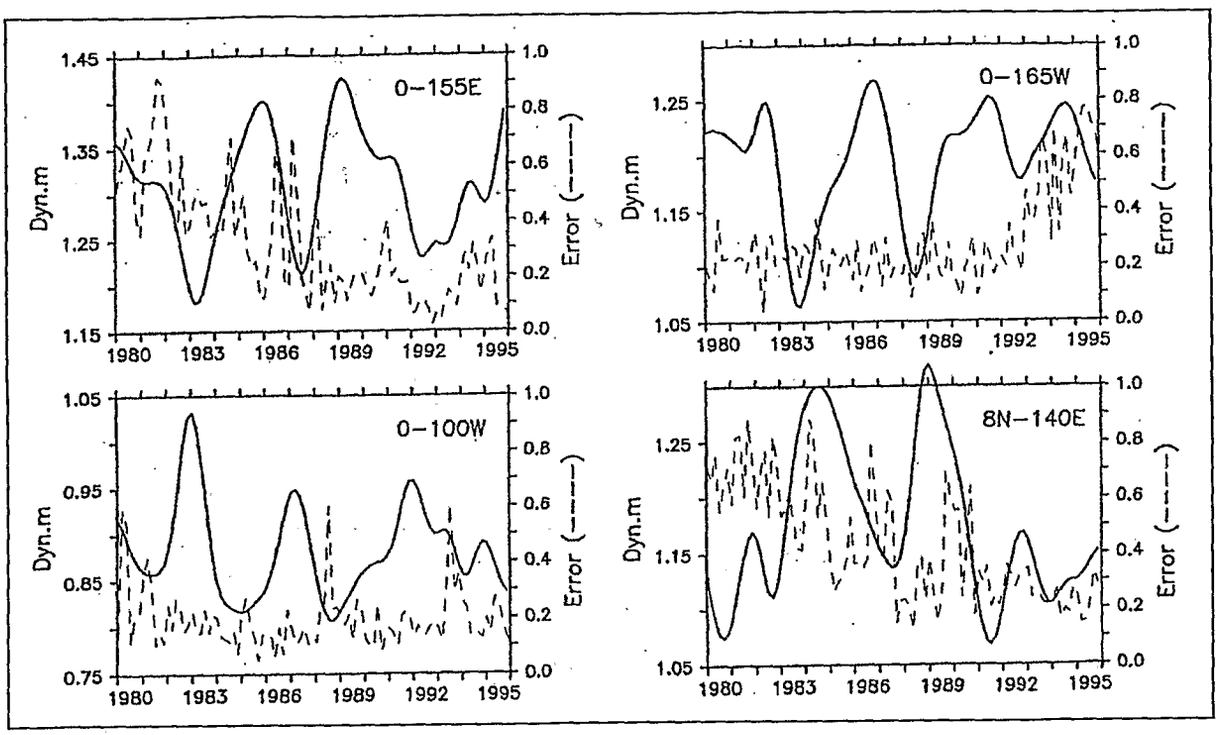

Figure 5. Interannual variations in 0/450 dbar dynamic height anomaly (full lines; left axes; dyn m) at a) 0°–155°E, b) 0–100°W, c) 0–165°W and d) 8°N–140°E. The dashed lines denote the estimated normalised errors (right axes).

SUMMARY AND CONCLUSION

The ENSO-related sea level changes are schematically concerned with two types of movements appearing somewhat like zonal and meridional "seesaws". The zonal "seesaw" concerns chiefly the equatorial band: it is characterised by anomalously low (high) sea level in the west lagging by about half a year behind anomalously high (low) sea level in the east during El Niño (La Niña). Interestingly, the sea level changes extend off the equator in the west reflecting the role of ENSO-related changes in the curl of the wind stress. The meridional "seesaw", which lags by about one year behind the SOI, consists of out-of-phase variations between the regions situated north and south of about 5°N, with the main changes happening in the western-central equatorial basin. The double "seesaws" result in a longitudinal mean sea level rise (drop) within about 5°N–20°S up to the mature phase, and not just till the beginning, of El Niño (La Niña), partly compensated by a longitudinal mean sea level drop (rise) within about 5°N–20°N.

The meridional sea level "seesaw", often described as regulating the pace of ENSO and in possible relation with its predictability, deserves further observational investigations in order to confirm or revise model interpretation. It would be appropriate to examine how water is redistributed at depths, and to distinguish the actual mechanisms at work. Still, this note focussed on the common large-scale sea level features rather than on individual characteristics of each El Niño and La Niña event. Clearly, the specificity of each event should be further analysed to improve our understanding of the ENSO-related sea level changes, particularly in the vicinity of low-level Pacific islands.

REFERENCES

Blackman, R. B. and Tukey, J. W. (1958). *The measurement of power spectra.* Dover publications Inc., New York, 190 pp.

Busalacchi, A., and O'Brien. J. (1981). Interannual variability of the equatorial Pacific in the 1960s. *J. Geophys. Res., 86,* 10901–10907.

Chao, Y., Halpern D. and Périgaud, C. (1993). Sea surface height variability during 1986–1988 in the tropical Pacific ocean. *J. Geophys. Res.,* 98, 6947–6959.

Chao, Y. and Philander, S. G. (1993). On the structure of the Southern Oscillation. *J. Climate, 6,* 450–469.

Delcroix, T., Eldin, G. and Hénin, C. (1987). Upper ocean water masses and transport in the western tropical Pacific (165°E). *J. Phys. Oceanogr., 17,* 2248–2262.

Enfield, D. and Cid, L. (1991). Low-frequency changes in El Niño Southern Oscillation. *J. Climate, 4,* 1137–1146.

Goldenberg, S. and O'Brien, J. J. (1981). Time and space variability of tropical wind stress. *Mon Wea. Rev., 109,* 1190–1207.

Hayes, S., Mangum, L., Picaut, J., Sumi, A. and Takeuchi, K. (1991). TOGA–TAO: a moored array for real time measurements in the tropical Pacific. *Bull. Am. Meteorol. Soc., 72,* 339–347.

Levitus, S., Burgett, R. and T. P. Boyer. (1994). *World Ocean Atlas 1994, Volume 3; Salinity.* NOAA Atlas, NESDIS 3, U.S. Dept. of Commerce, Washington, D.C., 97 pp.

McPhaden, M. and Taft, B. (1988). Dynamics of seasonal and intraseasonal variability in the eastern equatorial Pacific. *J. Phys. Oceanogr., 18,* 1713–1732.

McPhaden, M. (1993). TOGA–TAO and the 1991–93 El Niño Southern Oscillation event. *Oceanography, 6,* 36–44.

Meyers G., Phillips, H., Smith, N. and Sprintall, J. (1991). Space and time scales for optimal interpolation of temperature—Tropical Pacific Ocean. *Progr. Oceanogr., 28,* 189–218.

Pares-Sierra, A., Inoue, M. and O'Brien, J. (1985). Estimates of oceanic horizontal heat transport in the tropical Pacific. J. *Geophys. Res., 90,* 3293–3303.

Philander, S. and Hurlin, W. (1988). The heat budget of the tropical Pacific ocean in a simulation of the El Niño of 1982–83. *J. Phys. Oceanogr., 18,* 926–931.

Rébert, J. P., Donguy, J. R., Eldin G. and Wyrtki, K. (1985). Relations between sea level, thermocline depth, heat content, and dynamic height in the tropical Pacific. *J. Geophys. Res., 90,* 11719–11725.

Reid, J. (1961). On the geostrophic flow at the surface of the Pacific ocean with respect to the 1000 dbar surface. *Tellus, 13,* 489–502.

Springer, S., McPhaden, M. and Busalacchi, A. (1990). Oceanic heat content variability in the tropical Pacific during the 1982–83 El Niño. *J. Geophys. Res., 95,* 22,089–22,101.

Sverdrup, S. (1947). Wind-driven currents in a baroclinic ocean with application to the equatorial currents of the eastern Pacific. *Proc. Natl. Acad. Sci, 33,* 318–326.

Trenberth, K. (1984). Signal versus noise in the Southern Oscillation. *Mon. Wea. Rev., 112,* 326–332.

White W., Meyers, G., Donguy, J. R. and Pazan, S. (1985). Short-term climatic variability in the thermal structure of the Pacific Ocean during 1979–82. *J. Phys. Oceanogr., 15,* 917–935.

Wyrtki, K. (1977). Sea level during the 1972 El Niño. *J. Phys. Oceanogr., 7,* 779–787.

Wyrtki, K. (1985). Water displacements in the Pacific and the genesis of El Niño cycles. *J. Geophys. Res., 90,* 7129–7132.

Zebiak, S. and Cane, M. (1987). A model El Niño Southern Oscillation. *Mon Wea. Rev., 115,* 2262–2278.

Zebiak, S. (1989). Oceanic heat content variability and El Niño cycles. *J. Phys. Oceanogr., 19,* 475–486.